

# Regional now- and forecasting for data reported with delay: A case study in COVID-19 infections

Giacomo De Nicola<sup>\*</sup>, Marc Schneble<sup>\*</sup>, Göran Kauermann<sup>\*</sup> and Ursula Berger<sup>\*\*</sup>

<sup>\*</sup>Department of Statistics, Ludwig-Maximilians-University Munich, Germany

<sup>\*\*</sup>Institute for Medical Information Processing, Biometry and Epidemiology, Ludwig-Maximilians-University Munich, Germany

November 10, 2021

## Abstract

Governments around the world continue to act to contain and mitigate the spread of COVID-19. The rapidly evolving situation compels officials and executives to continuously adapt policies and social distancing measures depending on the current state of the spread of the disease. In this context, it is crucial for policymakers to have a firm grasp on what the current state of the pandemic is as well as to have an idea of how the infective situation is going to unfold in the next days. However, as in many other situations of compulsorily-notifiable diseases and beyond, cases are reported with delay to a central register, with this delay deferring an up-to-date view of the state of things. We provide a stable tool for monitoring current infection levels as well as predicting infection numbers in the immediate future at the regional level. We accomplish this through nowcasting of cases that have not yet been reported as well as through forecasting of future infections. The two steps are also combined in forenowcasting. We apply our model to German data, for which our focus lies in explaining and predicting infectious behaviour by district, age group and gender.

**- preliminary version, submitted to the  
International Journal of Forecasting -**

# 1 Introduction

The infectious disease known as COVID-19 hit the planet in tsunami-like fashion. The first cases were identified in December 2019 in the city of Wuhan, China, and by March 2020 infections had already spread over the entire world. Nearly all of the affected countries progressively implemented measures to slow down the spread of the virus, ranging from recommended social distancing to almost complete lockdowns of social and economic activity. These measures eventually proved to be effective, as the number of infections could be slowed down (see e.g. Flaxman et al., 2020 and Roux et al., 2020). This allowed numerous states to relax restrictions, in an attempt to gradually return to normality. At the same time, with the threat posed by the virus still looming, decision makers are forced to strike a balance between epidemiological risk and allowance of socio-economic activity. In this context, surveillance of the number of new infections is becoming increasingly important, and particularly so on a regional level. Given the local nature of the phenomenon (see e.g. Gatto et al., 2020 and Li et al., 2020), such regional view appears to be of crucial importance. One of the difficulties lies in the fact that exact numbers of infections detected on a particular day are only available with a reporting delay of, in some cases, several days, which occurs along the reporting line from local health authorities to the central register. The following paper provides a stable tool for monitoring current infection levels corrected for incompleteness of the data due to a reporting delay. This approach is also extended towards predicting the infectious behaviour in the immediate future at the regional level.

More specifically, the scope of our model is threefold: Firstly, we aim to understand the current epidemiological situation as well as to comprehend the association between the number of detected infections and demographic characteristics and geographical location. Secondly, our goal is to nowcast infections that have already been observed but have not yet been included in the official numbers. New infections are detected through tests and registered by the local health authorities, which in turn will report the numbers to national authorities with an inevitable delay. Since we observe reports of infections for each day, we are able to model this delay, which indeed allows to nowcast infection numbers for today correcting for infections which have not yet been reported. Lastly, our aim is also to forecast the epidemiological situation for the immediate future. We here want to stress that our model is not aiming to exactly predict future infection numbers, as that would not be realistic. The goal is rather to try and give a general idea of what is going to happen in the next few days in the different districts, and, perhaps most importantly, help identify which districts are going to be the most problematic. This could also help policymakers in making decisions regarding the implementation of safety measures at the regional level.

We apply our modelling approach to explain and predict numbers of registered COVID-19 infections for Germany by district, age group and gender. While the regional component

is of evident and paramount importance, the age group and gender distinctions are also very relevant, given the powerful interaction of demography and current age-specific mortality for COVID-19 (Dowd et al., 2020).

The statistical modelling of infectious diseases is a well developed scientific field. We refer to Held et al. (2017) for a general overview of the different models. Modelling and forecasting COVID-19 infections has been tackled by numerous research groups using different models. Panovska-Griffiths (2020) discusses whether one or multiple models may be useful for COVID-19 data analytics. Stübinger and Schneider (2020) make use of time warping to forecast COVID-19 infections for different countries (see also Cintra et al., 2020), while Dehesh et al. (2020) utilize ARIMA time series models. Early references during the first stages of the pandemic are Anastassopoulou et al. (2020) and Petropoulos and Makridakis (2020). In this paper we make use of Negative Binomial regression models implemented in the `mgcv` package in R. This allows us to decompose the spatial component in depth, and obtain district-level nowcasts and forecasts for Germany. One of our intentions is to demonstrate that today's "off the shelf" software can cope with the problem in an efficient as well as flexible way once the modelling problem has been defined in a suitable form. Our results confirm the dynamic and highly local nature of outbreaks, highlighting the need for continuous regional surveillance on a small area level.

The rest of the paper is structured as follows: Section 2 describes the data, while Section 3 frames the problem and presents our model. Section 4 describes how nowcasting and forecasting are performed, and Section 5 relates to model evaluation. Finally, Section 6 concludes the paper, highlighting the limitations of this study and adding some concluding remarks.

## 2 Data

As previously anticipated, we focus our analyses on German data. To do so, we make use of the COVID-19 dataset published by the Robert-Koch-Institute on a daily basis. The Robert-Koch-Institute (RKI) is a German federal government agency and scientific institute responsible for health reporting and for disease control and prevention. It maintains the national register for COVID-19, where all identified cases of this compulsorily-notifiable disease are reported from the local health authorities to the RKI. We have daily downloads of the data at our disposal, starting from March 27, 2020 until July 13, 2020. As we want our modelling to be dynamic, the surveillance analysis is performed considering only infections with registration dates within 21 days of the day of analysis, with earlier data allowing us to compare the differences in model fit over time.

Table 1 shows an exert of the data we are confronted with. Every morning, the database

Data downloaded on June 25, 2020	District (Landkreis)	Age Group (Altersgruppe)	Gender (Geschlecht)	Infections (Anzahl Fall)	Registration Date (Meldedatum)	Reporting Date (Datenstand)
	⋮	⋮	⋮	⋮	⋮	⋮
	Munich City	60-79	F	3	June 22, 2020	June 25, 2020
	Munich City	60-79	M	5	June 22, 2020	June 25, 2020
	⋮	⋮	⋮	⋮	⋮	⋮
Data downloaded on June 26, 2020	District	Age Group	Gender	Infections	Registration Date	Reporting Date
	⋮	⋮	⋮	⋮	⋮	⋮
	Munich City	60-79	F	6	June 22, 2020	June 26, 2020
	Munich City	60-79	M	5	June 22, 2020	June 26, 2020
	⋮	⋮	⋮	⋮	⋮	⋮

Table 1: Illustration of the raw data structure, showing downloads of the data from June 25 and June 26, 2020 as an example. To facilitate reproducibility, the original column names used in the RKI datasets are given in brackets below our English notation.

containing all registered COVID-19 infections is updated and released to the public, downloadable from the Robert-Koch-Institute’s repository<sup>1</sup>. The dataset contains, for each of the 412 districts, the cumulated number of confirmed cases of COVID-19 infections stratified by age group (00-04, 05-14, 15-34, 35-59, 60-79 or 80+) and gender (updated to that day), as well as the date of registration of each case by the local public health authorities (*Gesundheitsämter*). Through the merging of daily downloads of this RKI report, we can construct the full dataset as sketched in Table 1, where the release date is defined in the column “Reporting Date”. This full data format is necessary to trace the reporting delay for each observation. It can sometimes indeed take several days for the data to get from the local health authorities to the nation-wide central one, and we thus define reporting delay as the number of days between registration date and reporting date. Note that since the RKI reports data every morning, all reported cases will have a delay of at least one day. The delay is especially high during weekends, a fact that we take into account in our model. Due to the delayed nature of reporting, the number of registered COVID-19 cases which refer to a specific registration date might change with the reporting date, as exemplified in Table 1. On June 25, the RKI has reported three registered infections of females in the age group from 60-79 living in the city of Munich, which were registered on June 22, 2020. Due to delayed reporting, this number increased to six in the report of June 26, 2020. The three newly reported cases have therefore been reported with a delay of four days. Note once again that the RKI dataset available for download only contains the information up to the current date, thus making daily downloads of the datasets necessary to determine

<sup>1</sup><https://www.arcgis.com/home/item.html?id=f10774f1c63e40168479a1feb6c7ca74>

reporting delay.

For the sake of brevity, we here do not provide general descriptive statistics of the data, since these numbers can be easily obtained from many other sources. Among others, we refer to the RKI webpage<sup>2</sup>, which also includes a dashboard to visualize the data (see also CoronaMaps<sup>3</sup>).

## 3 Surveillance Model

### 3.1 Framing

We start motivating the model by first reformulating the data structure in a way that is suitable for the analysis. Let  $N_{t,d}$  denote the newly registered infections at day  $t$  which are reported with delay  $d$  and hence included in the database from day  $t + d$ . The minimum possible delay is one day, and we assume the maximum delay to be equal to  $d_{max}$  days. In our analysis we set  $d_{max} = 7$ , which corresponds to a week. In other words, we assume delayed reporting to happen within a week. If we define  $T$  as the time point of the analysis, the data available at that moment will take the form shown in Table 2. The bottom right triangle of the data is missing, so that the structure of the available data is akin to that of a guillotine blade. This comparison can be helpful to understand prediction of future values, since predicting by reporting date corresponds to making the blade fall down by one or more days. In other words, one of our goals will be to predict the diagonal edge of the blade, which corresponds to the predicted cases reported on day  $T + 1$ . To better explain our prediction strategy, we give a sketch of this idea in Figure 1. In the sketch, the green dots represent data that are already observed at time  $T$  (the day of analysis), while the crosses represent entries that are not yet observed and that we aim to predict with our model. This is done in three steps, which are described below. To be specific, we pursue *nowcasting*, *forecasting* and the combination of both, *forenowcasting*.

**Nowcasting** Since each row of the matrix contains cases registered on a single date, to obtain the amount of cases registered on that day, regardless of the delay with which they are reported, we need to take the sum of the corresponding row. If the goal is to obtain predictions by registration date for several days, we then just sum the cases over the corresponding rows. In Figure 1 we highlight this type of prediction with a green square, which represents a weekly nowcast, that is the number of cases with registration dates over

---

<sup>2</sup>[https://www.rki.de/EN/Home/homepage\\_node.html](https://www.rki.de/EN/Home/homepage_node.html)

<sup>3</sup><https://corona.stat.uni-muenchen.de/maps>

t	d			
	1	2	$\dots$	$d_{max}$
1	$N_{1,0}$	$N_{1,1}$	$\dots$	$N_{1,d_{max}}$
2	$N_{2,0}$	$N_{2,1}$	$\dots$	$N_{2,d_{max}}$
$\vdots$	$\vdots$	$\vdots$	$\vdots$	$\vdots$
$T - d_{max}$	$N_{T-d_{max},0}$	$N_{T-d_{max},1}$	$\dots$	$N_{T-d_{max},d_{max}}$
$T - d_{max} + 1$	$N_{T-d_{max}+1,0}$	$N_{T-d_{max}+1,1}$	$\dots$	NA
$\vdots$	$\vdots$	$\vdots$	$\vdots$	$\vdots$
$T - 1$	$N_{T-1,0}$	$N_{T-1,1}$	NA	NA
$T$	$N_{T,0}$	NA	NA	NA

Table 2: Reformulated data structure for a single district, age group and gender, explicitly including delay.

the past week. This comprises numbers that have already been observed as well as the predictions for cases from past days that have not yet been reported.

**Forecasting** If we shift the focus from predicting by registration date to reporting date, that is, if the aim is to predict reported numbers regardless of when the reported infections were actually first discovered, we cannot sum the entries of the matrix row-wise, but we need to do so diagonally. This is because the reported number on day  $T$  is comprised of the sum of cases registered on day  $T - 1$  reported with delay 1, cases registered on day  $T - 2$  reported with delay 2, and so on and so forth, up until cases registered on day  $T - d_{max}$  reported with delay  $d_{max}$ . The red parallelogram in Figure 1 thus represents the cumulated weekly forecast, that is, the predicted number of infections to be reported over the next seven days. Here all entries are unobserved, and will need to be predicted through our model, which will be uncovered in the following section.

**Forenowcasting** We can also combine the two aspects and predict the number of infections that will happen in the next week, regardless of their reporting date. This corresponds to the blue square in Figure 1 and in fact is a combination of forecasting and nowcasting.

We will demonstrate that the three types of predictions can be carried out with a single model, where predictions refers to extending the data row-wise (i.e. nowcasting), column-wise (i.e. forecasting) or both (i.e. forenowcasting).

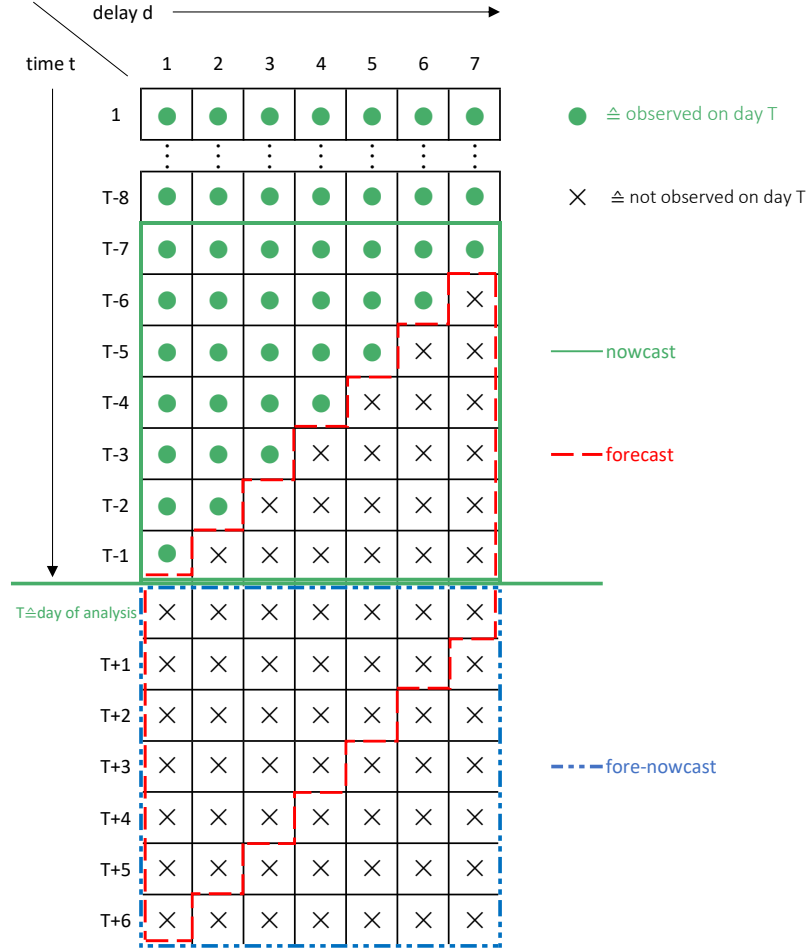


Figure 1: Sketch of the reformulated data structure showing how nowcasting, forecasting and forenowcasting are performed.

### 3.2 Statistical Model

As already stated in Section 2, the cumulative numbers of registered COVID-19 infections are, other than by registration date, also stratified by district, age group and gender. To accommodate this additional information, we extend the notation from above and define

with  $N_{t,d,r,g}$  the number of newly registered infections on day  $t$  in region/district  $r$  and gender and age group  $g$ , reported by the RKI on day  $t + d$  (thus with delay  $d$ ). Row-wise cumulated numbers are defined through

$$C_{t,d,r,g} = \sum_{j=1}^d N_{t,j,r,g} \quad (1)$$

which represents the group- and district-specific cumulated number of cases with registration date  $t$  and delay up to  $d$ . We define with  $\mathbf{z}_r$  the geo-coordinates of district/region  $r$  and generally denote covariates with  $\mathbf{x}$ , where varying subscripts indicate dependence on either gender- and age group  $g$ , region  $r$ , time point  $t$  or delay  $d$ .

We assume the counts  $N_{t,d,r,g}$  to follow a negative binomial distribution with mean  $\mu_{t,d,r,g}$  and variance  $\mu_{t,d,r,g} + \theta\mu_{t,d,r,g}^2$ , where  $\theta > 0$  and the limit  $\theta \rightarrow 0$  leads to a Poisson distribution. More specifically, we set

$$\begin{aligned} \mu_{t,d,r,g} = & \exp\{s_1(t) + s_2(\mathbf{z}_r) + \gamma_d + \mathbf{x}_{t,d}\boldsymbol{\alpha} + \mathbf{x}_g\boldsymbol{\beta} + \mathbf{x}_t\mathbf{u}_r + \\ & + \phi \log(1 + C_{t-1,d,r,g}) + \delta \log(1 + C_{t,d-1,r,g}) + \text{offset}_{r,g}\} \end{aligned} \quad (2)$$

Here,  $s_1(t)$  is a global smooth time trend and  $s_2(\mathbf{z}_r)$  is a smooth spatial effect over the districts of Germany. The parameters  $\boldsymbol{\gamma}_d = (\gamma_1, \dots, \gamma_{d_{max}})$  capture the delay effect for each delay  $d$  while the parameters contained in  $\boldsymbol{\alpha}$  capture effects related to time and delay, which in our case will be weekday effects. Gender and age effects are included in  $\boldsymbol{\beta}$ , and  $\mathbf{u}_r$  are unstructured regional effects which will be subsequently specified in more detail. Coefficient  $\phi$  captures the autoregressive component of the process, indicating the effect of cases from the same district and gender- and age group which were reported on the previous day. Coefficient  $\delta$  expresses the effect of infections registered on the same day which were reported with delay up to  $d - 1$ . Finally, the offset is set to the logarithm of the regional population size in the different gender- and age-groups, enabling us to model the infection rate. The offset defined this way also allows to incorporate the size of the susceptible population in each region. This shows that the type of modelling is practicable at different stages of the pandemic. In this case, the population size would need to be replaced by the number of susceptible in region  $r$ , incorporating the SIR (susceptible-infected-removed) model or other similar ones (see e.g. Allen, 1994). This is not particularly relevant at the time point of the analysis, since the number of susceptible corresponds more or less to the population size due to the small (and unknown) size of the immune populations in each district.

The previously mentioned spatial effect is comprised of two components: An overall smooth effect  $s_2(\mathbf{z}_r)$  mirroring the fact that different parts of Germany are differently



affected, and a region-specific component accounting for infection rates that are particularly high or low in single districts with respect to the neighbouring situation. To be more specific,  $s_2()$  is a smooth spatial function of the geo-coordinates  $\mathbf{z}_r$  for region  $r$ , while the  $\mathbf{u}_r$  are unstructured region-specific effects, interacting with the time dependent covariates  $\mathbf{x}_t$ . We put a normal prior on  $\mathbf{u}_r$ , i.e. we model  $\mathbf{u}_r = (u_{r0}, u_{r1})^\top$  as random effects, where  $u_{r0}$  is a general random intercept capturing the long-term level (from  $t = 1, \dots, T$ ) of the epidemiological situation in the different districts, while  $u_{r1}$  is a second random intercept estimated exclusively over the last  $k$  days, expressing the short-term dynamics (within  $k$  days prior to  $t = T$ ) of infections. In our analysis we set  $k = 7$ . For  $\mathbf{u}_r$  we assume the structure

$$\mathbf{u}_r \stackrel{iid}{\sim} N(\mathbf{0}, \Sigma_u) \quad (3)$$

for  $r = 1, \dots, 412$ , with the posterior variance matrix  $\Sigma_u$  being estimated from the data. The predicted values  $\hat{\mathbf{u}}_r$  (i.e. the posterior mode) measure how much and in which direction the infection rate of each district deviates from the global spatial structure, controlling for covariates and age- and gender-specific population sizes.

## 4 Results

Given that what we propose is a monitoring tool, the results change over time. We here give a snapshot of the estimates and predictions obtained using Monday, June 29, 2020 as date of the analysis providing predictions as well as infection numbers observed *a posteriori*, enabling comparison and model evaluation. As an additional remark, note that our analysis is completely reproducible for different dates as well, with code and data openly available and downloadable from our GitHub repository<sup>4</sup>.

### 4.1 Disease Monitoring

Table 3 shows the estimated linear coefficients resulting from the fitting of the model proposed in (3.2) estimated with data available on June 29, 2020. Note that the table here only shows the coefficients for the model fitted using data from the three weeks prior to that date, so all results are to be taken relatively to that period. A more complete and nuanced analysis of the evolution of the effects of covariates over time can be found in the Appendix. From the age-specific coefficients, we can see that there is some variability in the rates of reported cases in different age-groups. More specifically, we detect a lower rate of reported cases in the older population groups. This goes in the opposite direction

---

<sup>4</sup><https://github.com/gdenicola/Now-and-Forecasting-COVID-19-Infections>

of what we saw during the earlier stages of the pandemic, where cases were detected in higher proportion among the elderly. We can also observe that there is a significant albeit rather small difference in reported numbers for males and females. Note that interactions between age categories and gender effects were not included in the model due to their non-significance. Regarding pure reporting-related effects, we see that the most common delay for reported cases is one day (the reference category), followed closely by a delay of two days (0.66 times as likely). The occurrence of higher delays drops steeply from that point on, with the most extreme case being a delay of 7 days, which is only approximately 0.01 times as likely when compared to a single day delay. We can also observe a relatively strong weekday effect for Sundays, during which on average only half the cases are reported when compared to Mondays (the reference category).

The model also includes smooth components fitted over time and space, which can be visualized in Figure 2. The left hand side shows the estimated infection rate over time for the three weeks prior to June 29, 2020. We notice how the rate of registered infections has been dropping until mid-June. In the following week, a very large number of cases were detected in an outbreak in slaughterhouses in the district of Gütersloh, leading to an erratic increase in newly registered COVID-19 infections. Since this outbreak hardly spread over to neighbouring districts, the rate dropped down again towards the end of June.

We now focus on the spatial components, as we believe they play an important role as an initial step towards surveillance of infections at the regional level. The map on the right hand side of Figure 2 visualizes the smooth spatial effect, estimated as a function of longitude and latitude, on the log scale. From the plot we can see how, at the time of the analysis, the region of North-Rhine Westphalia and the Berlin area are generally the most affected. The two maps in Figure 3 show the district-specific random effects, which depict the situation in single districts controlling for the smooth spatial effect, that is, in comparison to the average of the neighbouring areas. More specifically, the map on the left displays the overall district-specific long-range random intercept, depicting the relative infection situations in the 21 days prior to the day of analysis, while the map on the right hand side shows the additional short-term random intercept which enters the linear predictor only over the last 7 days, giving an idea of the more recent infection dynamics. We can thus see that, for example, the district of Gütersloh has had the most rapidly evolving number of cases in the 7 days prior to the day of analysis, reflecting the outbreak in slaughterhouses that happened in the region (Middleton et al., 2020). This second map can already be seen as a first way of monitoring infection dynamics: if a district has a very high 7-days random effect, it probably means that something is going on there that deserves further consideration. We will show more sophisticated tools for performing this type of analysis in the following subsections.

		Effect (s.e.)	$\exp\{\text{Effect}\} /$ Relative Risk
Intercept		-14.005 (0.069)	$8.27 \cdot 10^{-7}$
Patient related effects	Age 00-04	0.032 (0.062)	1.033
	Age 05-14	0.136 (0.048)	1.146
	Age 15-34	0.299 (0.037)	1.349
	Age 60-79	-0.727 (0.049)	0.483
	Age 80+	-0.135 (0.060)	0.874
	Female	-0.117 (0.029)	0.890
Reporting related effects	Delay 2	-0.408 (0.033)	0.665
	Delay 3	-1.936 (0.051)	0.144
	Delay 4	-2.459 (0.063)	0.086
	Delay 5	-3.773 (0.106)	0.023
	Delay 6	-4.571 (0.164)	0.010
	Delay 7	-4.653 (0.173)	0.010
	Tuesday	0.436 (0.056)	1.547
	Wednesday	0.605 (0.058)	1.831
	Thursday	0.384 (0.064)	1.468
	Friday	0.622 (0.069)	1.863
	Saturday	0.080 (0.079)	1.083
	Sunday	-0.674 (0.088)	0.510
Autoregressive components	$\log(\text{C.t.-1.d})$	0.437 (0.037)	1.548
	$\log(\text{C.t.d-1})$	-0.003 (0.039)	0.997

Table 3: Estimated fixed linear effects (standard errors in brackets) for the negative binomial model. Parameters and their standard errors are given on the log scale. To facilitate interpretation, the multiplicative effect is also given (on the exp scale). The reference group for age is 35-59, while the reference category for the weekdays is Monday.

## 4.2 Nowcasting

We now use our model to nowcast the missing observations from past days which have not yet been observed due to the reporting delay. This allows for a more complete picture of the current epidemiological situation. In our case, nowcasting is equivalent to filling all NA (missing) entries of the matrix in Table 2, turning the trapezoid shape of the data into a full rectangle. This is also equivalent to completing the green square in Figure 1. Given

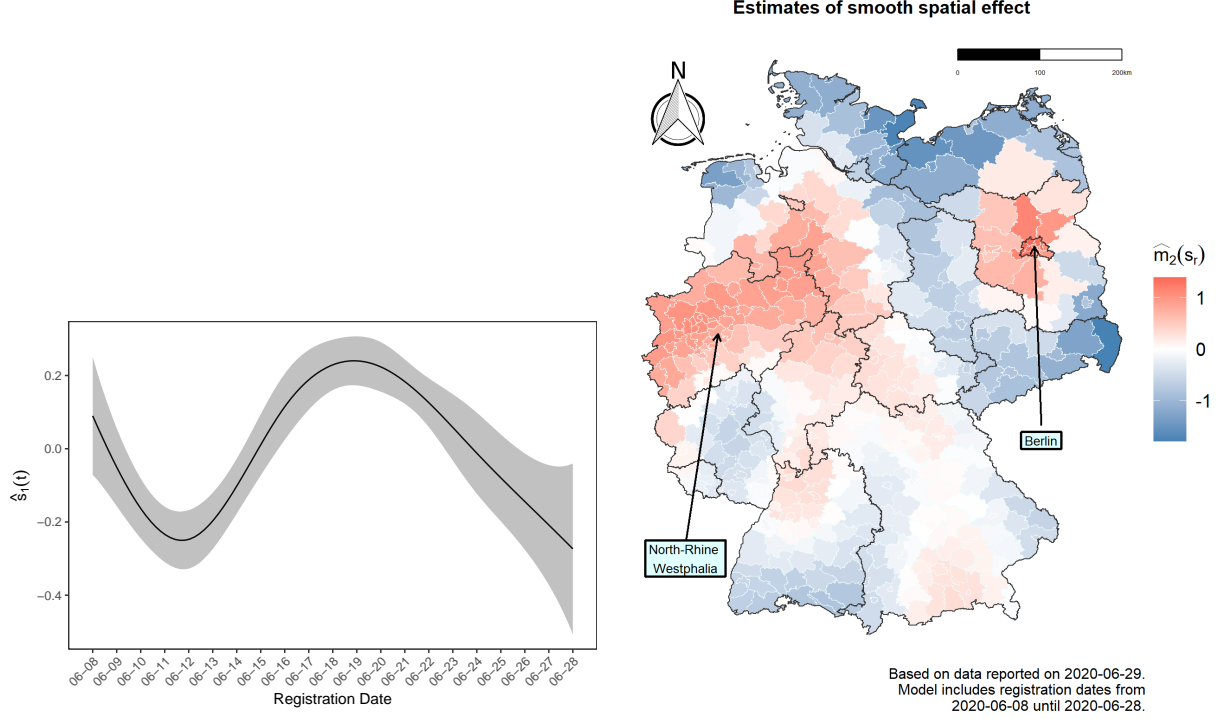


Figure 2: Estimated smooth effects  $s_1(t)$  and  $s_2(z_r)$ , respectively the fitted smooth effect of time and the fitted smooth spatial effect for the prevalence of COVID-19 infections in Germany (measured on the log scale). Both effects are estimated over the 21 days prior to June 29, 2020.

that we model delay as a stand-alone variable in our generalized additive model, we are able to simply predict the missing cells directly by setting the delay  $d$  to the necessary value in the data vector used for predictions alongside all other covariates. We can thus nowcast infections for each delay, day, district, gender and age group.

The predictions are also dependent on the autoregressive terms  $\log(1 + C_{t-1,d,r,g})$  and  $\log(1 + C_{t,d-1,r,g})$ . These are, except when predicting the first diagonal of the red parallelogram in Figure 1, not yet known at the day of analysis. We therefore perform the prediction of the black crosses in Figure 1 iteratively, by utilizing the predictions of the previous diagonal as the autoregressive components. Based on the model, we can also take uncertainty into account by simulating data from a negative binomial distribution

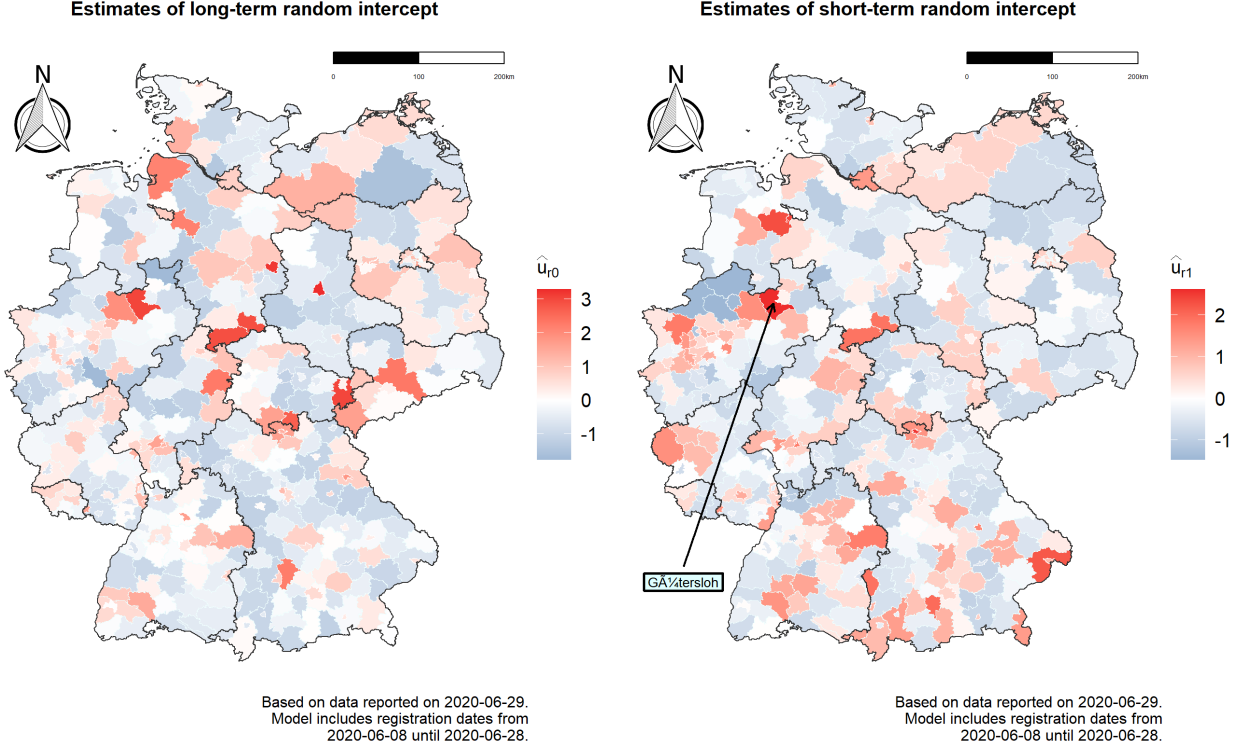


Figure 3: Region specific level (left) and dynamics (right) of COVID-19 infections, controlling for the spatial effect on the right hand side of Figure 2.

with the corresponding mean and variance structure. More precisely, we apply the same strategy as above, but instead of using the mean value we now plug counts simulated from the model into the autoregressive components, and repeat this procedure  $n = 1000$  times. This parametric bootstrap approach easily allows us to compute lower and upper bounds of the prediction intervals for nowcasting, forecasting and forenowcasting, which we show in Figure 4.

Setting  $d_{max} = 7$  we are able to compare the results of the nowcasts with realized infections a week after the analysis. The top panel of Figure 4 shows precisely that comparison, with cumulated nowcasted cases for the week from June 22 to June 28, 2020 using data available on June 29, 2020 for each district on the y axes and the corresponding realized cases, observed in full a week later, on the x axes. Vertical lines indicate prediction intervals at the 90% level. From the plot we can observe how the nowcasts are able to capture most of the residual variability in the data, including that for the aforementioned district of Gütersloh, in which the outbreak was ongoing. The biggest error in the nowcast is observed

for the district of Oldenburg, in which apparently an anomalously large number of cases were reported with delay. More detailed and quantitative measures of the quality of the nowcasts can be found in Section 5.

### 4.3 Forecasting

The model also allows to directly predict cases for future dates. With  $T$  denoting the time point of data analysis, we can obtain predictions for the number of reported cases on days  $T, T + 1, \dots, T + k - 1$ . Let us start with the predictions for the reported cases on the day of analysis, i.e. time  $T$ . Referring once again to the guillotine blade structure in Table 2, we proceed as follows: For  $d = 1$ , i.e. at the leftmost point of the blade, we take the mean value as prediction, while keeping the smooth function of time constant, that is, setting  $s(t + 1) \equiv s(t)$  for the sake of stability. For the remaining  $d_{max} - 1$  elements of the blade edge we take the mean value by setting  $d = d + 1$ . To get predictions for the numbers of infections reported on days  $T + 1, \dots, T + k - 1$  we can then proceed in an analogous way, using the values just predicted to update the autoregressive components ( $C_{t-1,d,r,g}$  and  $C_{t,d-1,r,g}$ ). Figure 1 visualizes the strategy, with cumulated predictions for the number of cases reported on days  $T, T + 1, \dots, T + 6$  being represented by the red parallelogram. Similarly as we did for the nowcasting, we can take uncertainty into account through simulations, sampling from a negative-binomial model with the estimated group-specific mean and variance structure.

We can compare the the predictions for the next  $k$  days with the realized reports after at least  $k$  days have passed. The bottom left panel of Figure 4 shows cumulated forecasts for cases reported during the week from June 29 to July 5, 2020 using data available on June 29, 2020. Predictions are reported on the y axes, while the corresponding realized reports, observed in full a week later, are on the x axes. Once again, vertical lines indicate prediction intervals at the 90% level. Overall, we can observe that the forecasts are predictably less accurate than the nowcasts, since there is much more uncertainty in the prediction of future cases, as sources of variability not yet known at the time of the analysis can appear in the data. Despite this, we can see that the outcome for the district of Gütersloh was predicted relatively accurately, with some overestimation possibly also resulting from restrictive social distancing measures imposed on the area after the outbreak was uncovered. A more quantitative take on the quality of the forecasts can be found in Section 5.

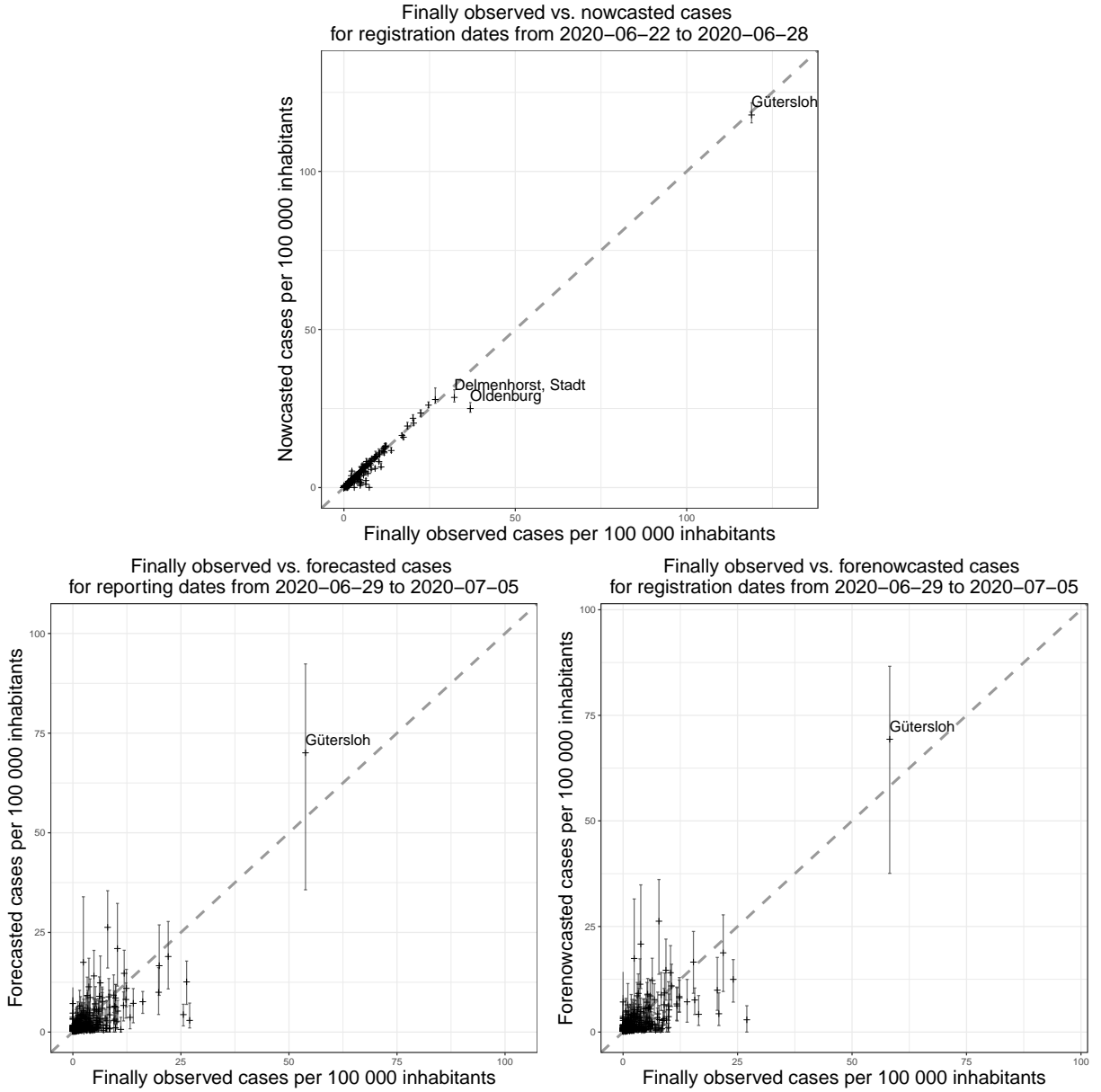


Figure 4: Nowcasts (top panel), forecasts (bottom left panel) and forenowcasts (bottom right panel) of cumulated infections over a week, cumulated by district, plotted against values observed *a posteriori*. The model is fitted with data available on June 29, 2020. Vertical lines represent prediction intervals computed at the 90% level.

## 4.4 Forenowcasting

The forecasts as we just defined them aim to predict the number of infections reported on certain dates. It is also possible to combine forecasting and nowcasting to predict cases by registration date, thus setting the real number of infections being discovered during a specific set of dates as target variable. This process, that we call *forenowcasting*, is equivalent to filling the blue square on the bottom of Figure 1. This is done by computing forecasts as described in the previous subsection, and then performing nowcasting on the forecasted numbers. We can also obtain uncertainty estimates in an analogous way as for forecasts and nowcasts.

Realizations of the forenowcasted cases can be observed after  $k + d_{max}$  days. The bottom right panel of Figure 4 shows how our forenowcasts performed with data available on June 29, 2020 compared to the corresponding numbers of infections finally observed for the week from June 29 to July 5, 2020. The results are once again cumulated by district, with vertical lines representing 90% prediction intervals. We can see that the results do not differ greatly from those of the forecasts previously shown, with some additional uncertainty being added by the variability in delayed reporting. Once again, quantitative measures of the quality of the predictions can be found in the following section.

## 5 Model Evaluation

In this section we assess the predictive accuracy of our model. To do so, we take a look at the cumulated realized prediction error with regards to nowcasts, forecasts and forenowcasts, for each district and over a period of seven days. Starting with nowcasting, let therefore  $Y_{T,r}^{(n)}$  denote the cumulated number of registered infections in district  $r$  over  $k = 7$  days prior to the day of analysis at time  $T$ , that is

$$Y_{T,r}^{(n)} = \sum_{t=1}^k \sum_g C_{T-t, d_{max}, r, g}$$

with  $C_{T, d_{max}, r, g}$  defined as in (1). This corresponds to the sum of all numbers in the green square in Figure 1. Accordingly, we define with  $\hat{Y}_{T,r}^{(n)}$  the corresponding prediction based on the fitted model as described above. For forecasting, we modify the definition and look at the cumulated number of cases

$$Y_{T,r}^{(f)} = \sum_{t=1}^k \sum_{d=1}^{d_{max}} \sum_g N_{T+t-d, d, r, g}$$



which corresponds to the red parallelogram in Figure 1. Again, the corresponding predicted value is notated as  $\widehat{Y}_{T,r}^{(f)}$ . Finally, for forenowcasting we concentrate on the cumulated numbers in the blue square, and set

$$Y_{T,t}^{(fn)} = \sum_{t=1}^k \sum_g C_{T+t-1,d_{max},r,g}$$

with matching prediction  $\widehat{Y}_{T,t}^{(fn)}$  based on the fitted model. With the notation just given, we can define the relative prediction error (standardized per 100.000 inhabitants) simply as

$$RPE_{T,r}^{(\cdot)} = 100.000 \frac{Y_{T,r}^{(\cdot)} - \widehat{Y}_{T,r}^{(\cdot)}}{pop_r}$$

where  $pop_r$  is the population size in district  $r$ , and the dot refers to nowcasting, forecasting or forenowcasting, respectively. It should be clear that the numbers defined above are only observable on day  $T+7$  for nowcasting and forecasting and on day  $T+14$  for forenowcasting.

Let us first take a look at the predictive accuracy of our model applied to nowcasting. The district-specific prediction error for nowcasting the week from June 22 to June 28, 2020 with data available on June 29, 2020 are shown in Figure 5. We plot  $RPE_{T,r}^{(n)}$ , where the districts  $r$  are ordered from left to right based on their population size. We can see that the prediction errors for the nowcasts are relatively close to the zero line, and apparently do not depend on the population size in the districts. We here labelled some of the biggest deviations, with the only real outlier being Oldenburg, for which there was a large amount of cases reported with substantial delay during the considered week.

We now turn our attention to prediction errors of future days. Once again, we make a distinction between predicting purely by reporting date (forecasting) and by registration date (forenowcasting, in our notation). Let us first focus on the forecast errors, which are shown in Figure 6. The forecast is performed using data available on June 29, 2020, and aims to predict cases to be reported during the week from June 29 to July 5, 2020. The variability here is noticeably much more considerable than in the nowcasting, which is not surprising since many more potentially unknown sources of variability can come into play in the future. Despite this, we can observe how the residuals are still quite evenly distributed around the zero line. We again highlighted the district for which the prediction error is larger, and we are especially interested in the districts for which the model underpredicted. For the considered week, the largest underprediction relatively to population size was for the district of Dingolfing-Landau in Bavaria, in which an outbreak in a joint accommodation for asylum seekers occurred unexpectedly. The second largest underprediction occurred for the district of Germersheim in the state of Rhineland-Palatinate, where there was also

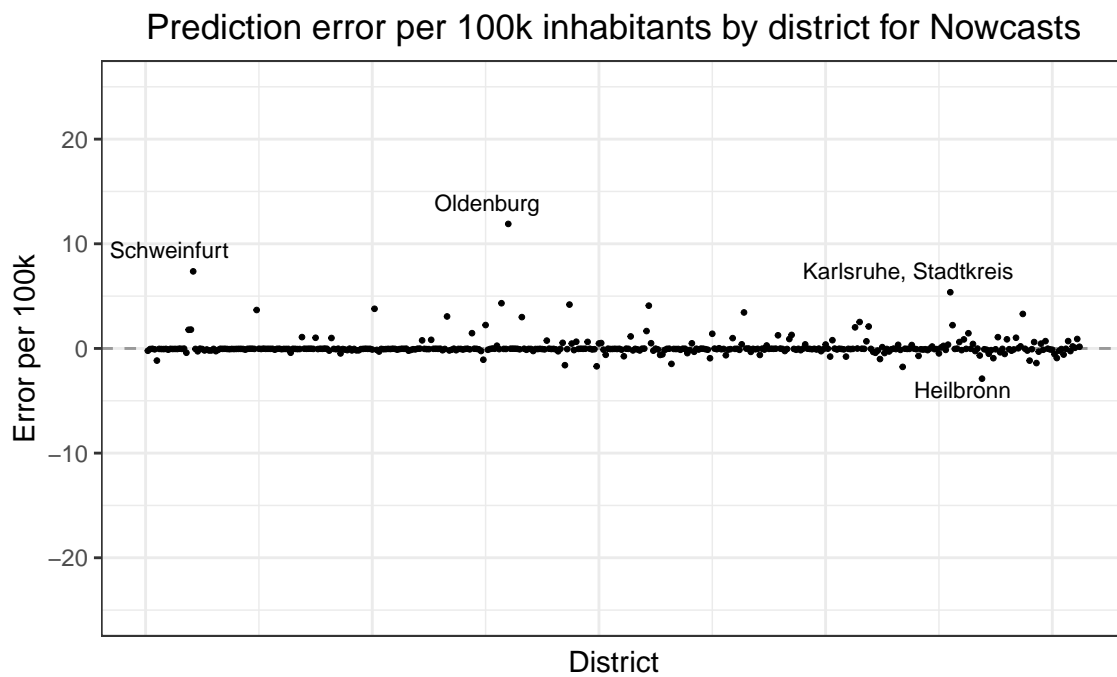


Figure 5: Prediction error for Nowcasts performed for the week from June 22 to June 28 with data available on June 29, 2020. Districts are shown in ascending order with respect to population size.

an outbreak, this time in relationship with a religious community. In general, the largest under-predictions will tend to be due to new outbreaks, which are still unknown at the time of the model estimation. While this can be considered as a limitation in our approach, severe underprediction can also be used *a posteriori* as an indicator of localized outbreaks. We discuss this point in Section 6. On the other hand, evident overpredictions are also related to recent outbreaks, which were already known at the time of the analysis and for which countermeasures were taken by the authorities to limit the spread. This is here the case for Coburg, where outbreaks in slaughterhouses had occurred in the weeks prior to the forecasting, with policymakers reacting accordingly. Newly enforced social distancing measures are exogenous to our model, which is thus destined to overpredict when the new rules start having an impact. While this is, in some sense, another limitation, it can also be viewed as a "feature" of our model: It provides a prediction of what would happen if no measures are taken, a counterfactual of some sort that can help us quantify the impact of changes in behaviour that happened following the outbreaks. This aspect will also be further discussed in the concluding section.

We finally turn our attention to the forenowcast prediction errors, namely the difference between the predicted cases to be registered during the week June 29 - July 5 with data available on June 29th, 2020 with the realized registered cases during that week observed two weeks later. The district-specific cumulated errors by 100 000 inhabitants are shown in Figure 7.

From the plot we can observe how the predictive performance for the forenowcasts is quite similar to that of the forecasts. The errors are again quite evenly distributed around zero, and do not seem to depend on population size. Two more districts are labelled (Delmenhorst and Bad Tölz-Wolfrathausen) which appear to have reported respectively an anomalously small and large number of infections with a delay.

To conclude this section, we also report the coverage of the prediction intervals graphically displayed in Figure 4. The coverage of the intervals, constructed for the 90% level for within-sample predictions and computed with 5000 simulations, is respectively 84.4% for the nowcast, 76.2% for the forecast and 76.7% for forenowcasting. Nowcast intervals predictably perform better, getting relatively close to nominal accuracy, while forecasting and forenowcasting intervals perform very similarly, showing that trying to predict more cells of cases reported with delay, namely "nowcasting the forecasts", does not seem to cost much in terms of predictive accuracy. While the undercoverage of the forecast and the forenowcast might look problematic, we do not believe this to be the case. As already mentioned, the model can not predict sudden outbreaks due to previously unknown sources of variability, be it in slaughterhouses or residential homes for asylum seekers. Severe under- and overpredictions can, as already argued, also be used to show that observed numbers are not explainable through past data, with underpredictions serving as an indica-

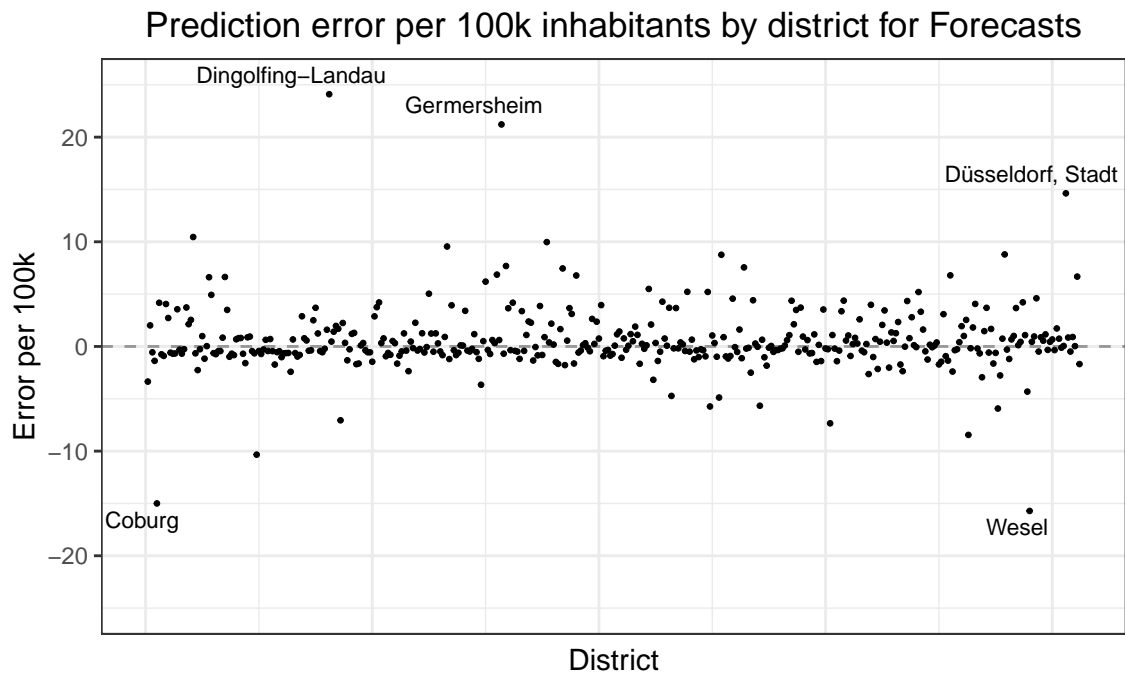


Figure 6: Prediction error for Forecasts performed for the week June 29-July 5 with data available on June 29, 2020. Districts are shown in ascending order with respect to population size.

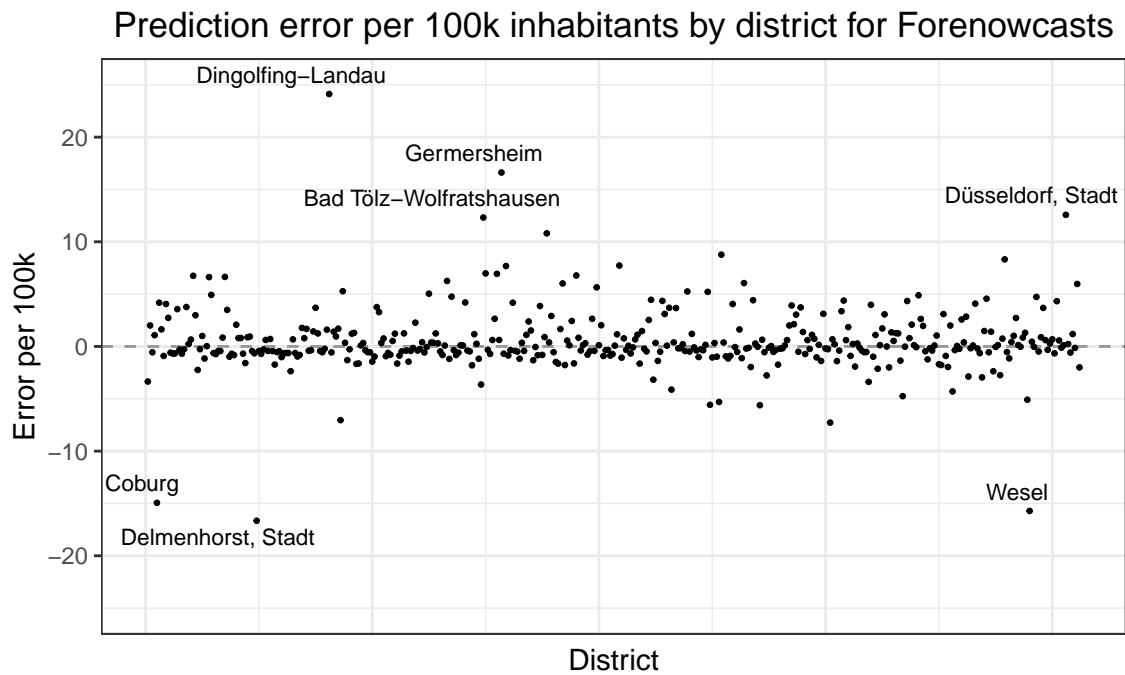


Figure 7: Prediction error for Forenowcasts performed for the week June 29-July 5 with data available on June 29, 2020. Districts are shown in ascending order with respect to population size.

tor for localized outbreaks and overpredictions signalling and quantifying the effectiveness of countermeasures.

## 6 Discussion

We proposed a numerically stable tool to nowcast and forecast COVID-19 cases reported with delay. This allows to perform surveillance by gender and age group at the regional level. As previously mentioned, this approach does not come without limitations, which we also want to address.

The number of detected cases greatly depends on local testing strategies and capacities. This implies that comparisons between different states or regions are not straightforward. As our model makes use of reported infections, nowcasting and forecasting results are also equally affected by this issue. Direct comparisons should thus be limited to areas for which it is reasonable to assume that testing has been carried out in a similar manner.

An eminent limitation of our approach is the inability to capture new outbreaks related to specific phenomena that are not yet known to the health authorities. An example of this would be the outbreak in slaughterhouses in Coesfeld, North Rhine-Westphalia. After all, of course, the model predicts future infections with data from the past, and is not clairvoyant. As previously discussed, severe underpredictions observed *a posteriori* can also be used as an indicator for outbreaks that are localized and not explainable by past data, while overpredictions can signal and quantify the effectiveness of social distancing measures. This last point is motivated by the fact that our model does not include anything regarding exogenous social distancing measures. This means that the predictions are to be interpreted assuming that everything else stays the same, leading to overprediction for areas in which measures are indeed imposed. On the other hand, this can also be seen as a feature of the model, which in a sense provides potential future "counterfactual" scenarios in which no action is taken by decision makers. A prime example of this is the prediction for the previously mentioned district of Gütersloh for the model fitted using data available on July 6, 2020, just a week later than the week we displayed. While the model predicted more than 1000 weekly cases per 100.000 inhabitants, a truly disastrous proposition, the realized number of infections in that week was just around 125 cases per 100.000, presumably thanks in large part to non-pharmaceutical interventions (NPI).

Taking into account the previously mentioned limitations, the model is able to capture a good chunk of the variability that is present. The methodology that we employed is quite general, and, if suitable data is available, can easily be adapted to other countries as well. Moreover, we only employed standard tools for software implementation, and this makes adapting and enriching the model, e.g. with more covariates, relatively straightforward.

We here did not include more covariates which would be available for the special case of Germany (e.g. district-wise deprivation indexes, see Maier, 2017), because we want our modelling exercise to be flexible and easy to apply to any country for which basic data is available. Nonetheless, it would most certainly be fruitful, at least from a predictive accuracy perspective, to include more covariates which are available for specific cases in the model.

We complete our discussion by emphasizing that the proposed methodology is flexible and applicable to any data constellation in which reporting delay plays a role. In other words, one can easily adopt the proposed model to any guillotine blade-like data structures, i.e. data where  $t_i$  denotes the time point of an event and  $d_i$  the delay with which the event is reported. Moreover, our approach can not only be applied to correct for the delay between registration of an event and its reporting, but also, for example, to bridge the delay between disease onset and registration of its positive test result. Data in guillotine blade-like form also occur in areas beyond epidemiology, e.g. when cases of unemployment are reported from regional offices to a central state register. The generality of the data structure supports the proposed modelling approach, where corrections for the missing data structure are directly incorporated in the model. In particular, however, the modelling exercise exhibits promising performance for COVID-19 infections, and may therefore be incorporated into a general surveillance tool to assist health authorities and policy makers in their efforts to contain the spread.

## Funding

This research did not receive any specific grant from funding agencies in the public, commercial, or not-for-profit sectors.

## References

- Allen, L. J. (1994). Some discrete-time si, sir, and sis epidemic models. *Mathematical Biosciences* 124(1), 83 – 105.
- Anastassopoulou, C., L. Russo, A. Tsakris, and C. Siettos (2020). Data-based analysis, modelling and forecasting of the covid-19 outbreak. *PLoS ONE* 15(3). <https://doi.org/10.1371/journal.pone.0230405>.
- Cintra, P., M. Citeli, and F. Fontinele (2020). Mathematical models for describing and predicting the covid-19 pandemic crisis. <https://arxiv.org/abs/2006.02507>.
- Dehesh, T., H. Mardani-Fard, and P. Dehesh (2020). Forecasting of covid-19 confirmed cases in different countries with ARIMA models. <https://doi.org/10.1101/2020.03.13.20035345>.
- Dowd, J. B., L. Andriano, D. M. Brazel, V. Rotondi, P. Block, X. Ding, Y. Liu, and M. C. Mills (2020). Demographic science aids in understanding the spread and fatality rates of covid-19. *Proceedings of the National Academy of Sciences* 117(18), 9696–9698.
- Flaxman, S., S. Mishra, A. Gandy, H. J. T. Unwin, T. A. Mellan, H. Coupland, C. Whitaker, H. Zhu, T. Berah, J. W. Eaton, M. Monod, Imperial College COVID-19 Response Team, A. C. Ghani, C. A. Donnelly, S. M. Riley, M. A. C. Vollmer, N. M. Ferguson, L. C. Okell, and S. Bhatt (2020). Estimating the effects of non-pharmaceutical interventions on COVID-19 in Europe. *Nature*, 1–8.
- Gatto, M., E. Bertuzzo, L. Mari, S. Miccoli, L. Carraro, R. Casagrandi, and A. Rinaldo (2020). Spread and dynamics of the covid-19 epidemic in italy: Effects of emergency containment measures. *Proceedings of the National Academy of Sciences* 117(19), 10484–10491.
- Held, L., S. Meyer, and J. Bracher (2017). Probabilistic forecasting in infectious disease epidemiology: The 13th armitage lecture. *Statistics in medicine* 36.
- Li, R., S. Pei, B. Chen, Y. Song, T. Zhang, W. Yang, and J. Shaman (2020). Substantial undocumented infection facilitates the rapid dissemination of novel coronavirus (sars-cov-2). *Science* 368(6490), 489–493.
- Liu, K., Y. Chen, R. Lin, and K. Han (2020). Clinical features of covid-19 in elderly patients: A comparison with young and middle-aged patients. *Journal of Infection* 80(6), e14 – e18.



- Ludvigsson, J. F. (2020). Systematic review of covid-19 in children shows milder cases and a better prognosis than adults. *Acta Paediatrica* 109(6), 1088–1095.
- Maier, W. (2017). Indices of multiple deprivation for the analysis of regional health disparities in germany : Experiences from epidemiology and healthcare research. *Bundesgesundheitsblatt Gesundheitsforschung Gesundheitsschutz* 60(12).
- Middleton, J., R. Reintjes, and H. Lopes (2020). Meat plants—a new front line in the covid-19 pandemic. *BMJ* 370.
- Panovska-Griffiths, J. (2020). Can mathematical modelling solve the current covid-19 crisis? *BMC Public Health*. <https://doi.org/10.1186/s12889-020-08671-z>.
- Petropoulos, F. and S. Makridakis (2020). Forecasting the novel coronavirus covid-19. *PLoS ONE* 15. <https://doi.org/10.1371/journal.pone.0231236>.
- Roux, J., C. Massonnaud, and P. Crépey (2020). Covid-19: One-month impact of the french lockdown on the epidemic burden. *medRxiv*.
- Stübinger, J. and L. Schneider (2020). Epidemiology of coronavirus covid-19: Forecasting the future incidence in different countries. *Healthcare* 8(2)(99). <https://doi.org/10.3390/healthcare8020099>.

# Appendix

## Evolution of covariates effect over time

In the main body of the paper we focused on explaining our model and how to use it to perform different types of predictions. In principle, it is also possible to make use of that same model in explanatory fashion, to gain insight on some of the dynamics of the pandemic. In this supplementary section we will go a little bit in this direction, focusing in particular on the changes in the effect of different covariates on the reported COVID-19 infections over time.

Given that we have daily downloads of the RKI dataset available from the very end of March onwards, we have a complete picture of the data (including the reporting delay) starting from after the first week of April. We then take into account the usual three weeks of data to be fed to our model, and fit ten different models a week apart from each other, with the first one having fitting date April 27, 2020 and the last one being fit on June 29th, 2020 (the latter being the same one that we showed throughout the paper). Our goal in this is that of comparing the estimated coefficients and observing their evolution over time. Let us start by looking at the Intercept (Figure 8).

The decreasing trend from the beginning of April is evident, with the intercept going from almost -12 to approximately -14, implying a decrease in the baseline relative risk for the reference group (males aged 36-59 living in the average district) of a whole order of magnitude (from  $6 \cdot 10^{-6}$  to  $8 \cdot 10^{-7}$ ). Nonetheless, we also observe how the decrease came to a halt starting from the end of May (given that each fitting date refers to the previous three weeks of data), with the risk of a confirmed infection for the reference group staying more or less constant throughout the month of June.

Next up we focus on how the effects for different age and gender groups evolved. The evolution of those coefficients is shown in Figure 9. The plot displaying the age group coefficients is in our opinion especially interesting, as the effects show considerable variation over time. This variation can apparently be interpreted: In the earlier stages of the pandemic, when there was a very high number of infections and testing was not yet as widespread in comparison to the prevalence of the disease, the older categories showed a much higher likelihood of getting a confirmed infection with respect to younger age-groups. This is because at the time testing was inevitably much more dependent on symptoms, and given that symptoms are very much age-dependent (see e.g. Dowd et al., 2020 and Liu et al., 2020), a higher number of cases is likely to have been detected among the elderly. This would also explain the low coefficients for the very young age groups, for which the likelihood of showing severe symptoms is lower (Ludvigsson, 2020). With the shrinking of the number of infections in Germany and the simultaneous rise in testing capacity over

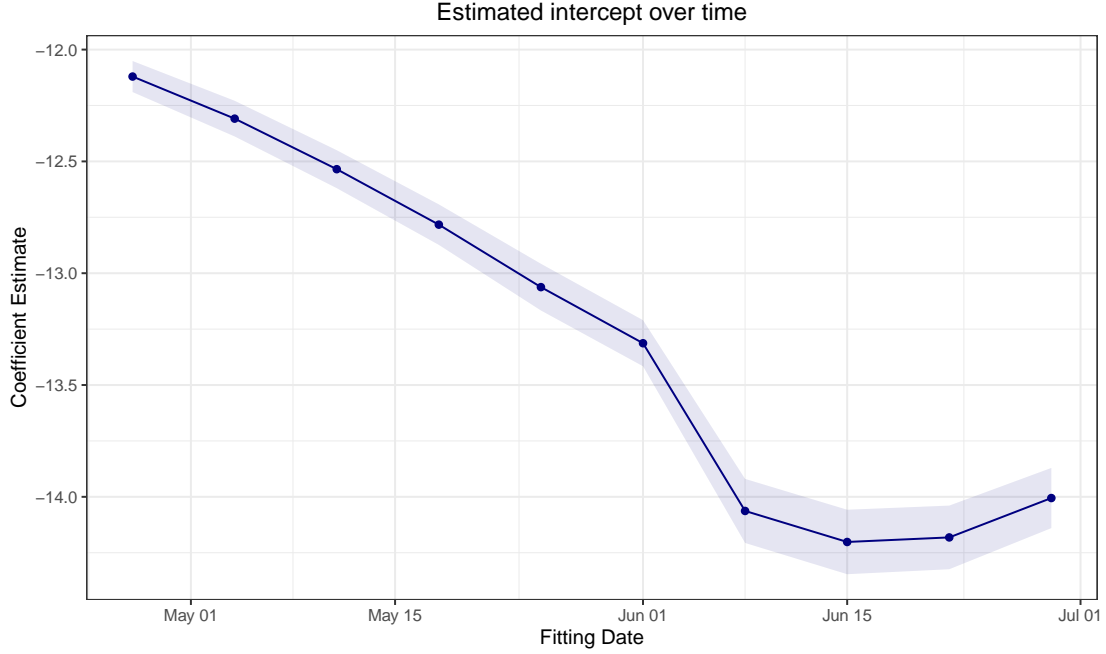


Figure 8: Estimated intercept over time, showing a decrease in relative risk for the reference category from April to June.

time, the dependency between testing and symptoms became much weaker, thus also gradually ironing out the differences between the detected cases in different age groups. We emphasize that all coefficients here are to be interpreted in relationship to the reference category, so the rise in the effects for ages 0-4 and 5-14 is absolutely not to be viewed as an increase in the prevalence for those age-groups, but rather only as a relative change in proportions. Switching our focus to the plot for the effect of gender, we see how, controlling for all other factors, variation in gender hardly affects the chance of suffering from a confirmed COVID-19 infection.

We next take a look at the coefficients for the two autoregressive components, namely that in  $C_{t-1,d,r,g}$  and the one in  $C_{t,d-1,r,g}$ . The former indicates the cases reported on the previous day in the same district and age- and gender-group with up to the same delay, while the latter stands for the number of cases reported on the same day, within the same district and age- and gender-group, but with a shorter delay. From the plot in Figure 10 we can see how the effects of those two components remained relatively stable over time, with the exception of the delay component practically losing its effect in the latest two weeks.

Finally, we focus on the behaviour of the reporting-related components of the model,

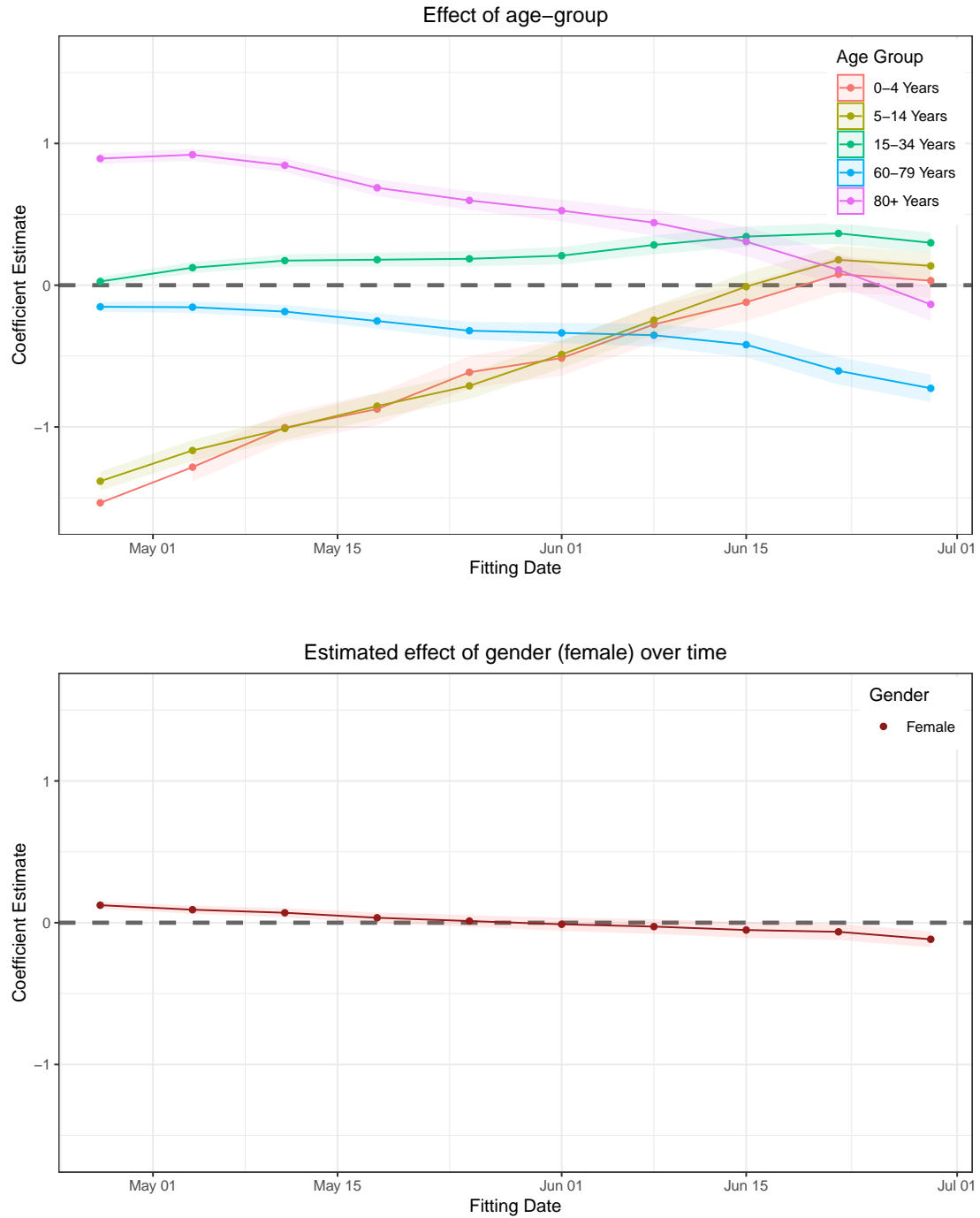


Figure 9: Estimated coefficients for the different age-groups and gender over time. The dashed zero line corresponds to the effect of the reference category (age group 35-59 years and male, respectively). Age group effects tend to converge over time, potentially indicating a progressively declining dependency of testing from symptoms.

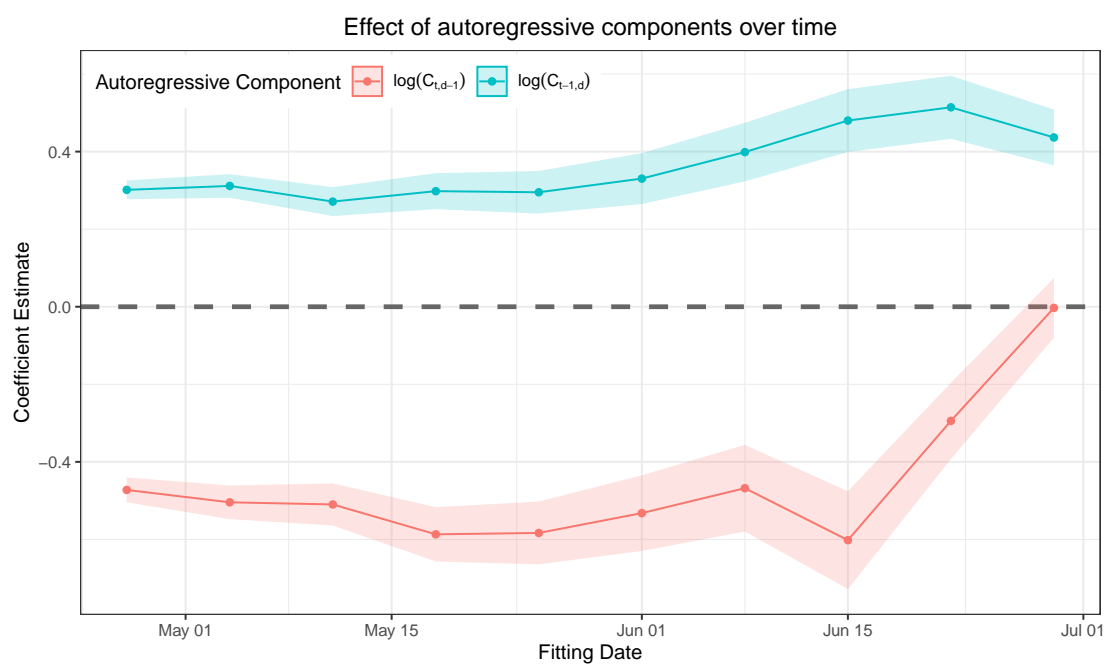


Figure 10: Estimated effects of the two autoregressive components of the model over time.

namely the effects of delay and weekday. The evolution of both of those is depicted in Figure 11. Looking at the plot for delay, we can appreciate how most of the coefficients decreased over time, showing an improvement in the reporting system leading to reduced delays. This is especially true for delay2 and delay3, indicating that more and more cases were reported from the national authorities only one day after they were registered by the local ones, as opposed to having a delay of two or three days. As a general consideration, we can appreciate how the delay components of the model remained relatively stable over time, with all coefficients remaining in decreasing order from the shortest delay to the longer one. Weekday effects are also comparatively stable over time, with reporting on Sunday being consistently lower than in all other days, and Saturday following suite as second to last. All other days of the week seem to be relatively similar with to each other with respect to reporting. A big change in the coefficients can be observed at the very beginning of the considered time window, when Easter Monday (April 14, 2020) was included in the data, thus making the effects of Saturday and Sunday go up with the respect to Monday (the reference category). A very similar phenomenon lead to the other large change in slope for most coefficients, at the beginning of June, with the holiday causing the change being in this case Pentecost Monday (June 1, 2020).

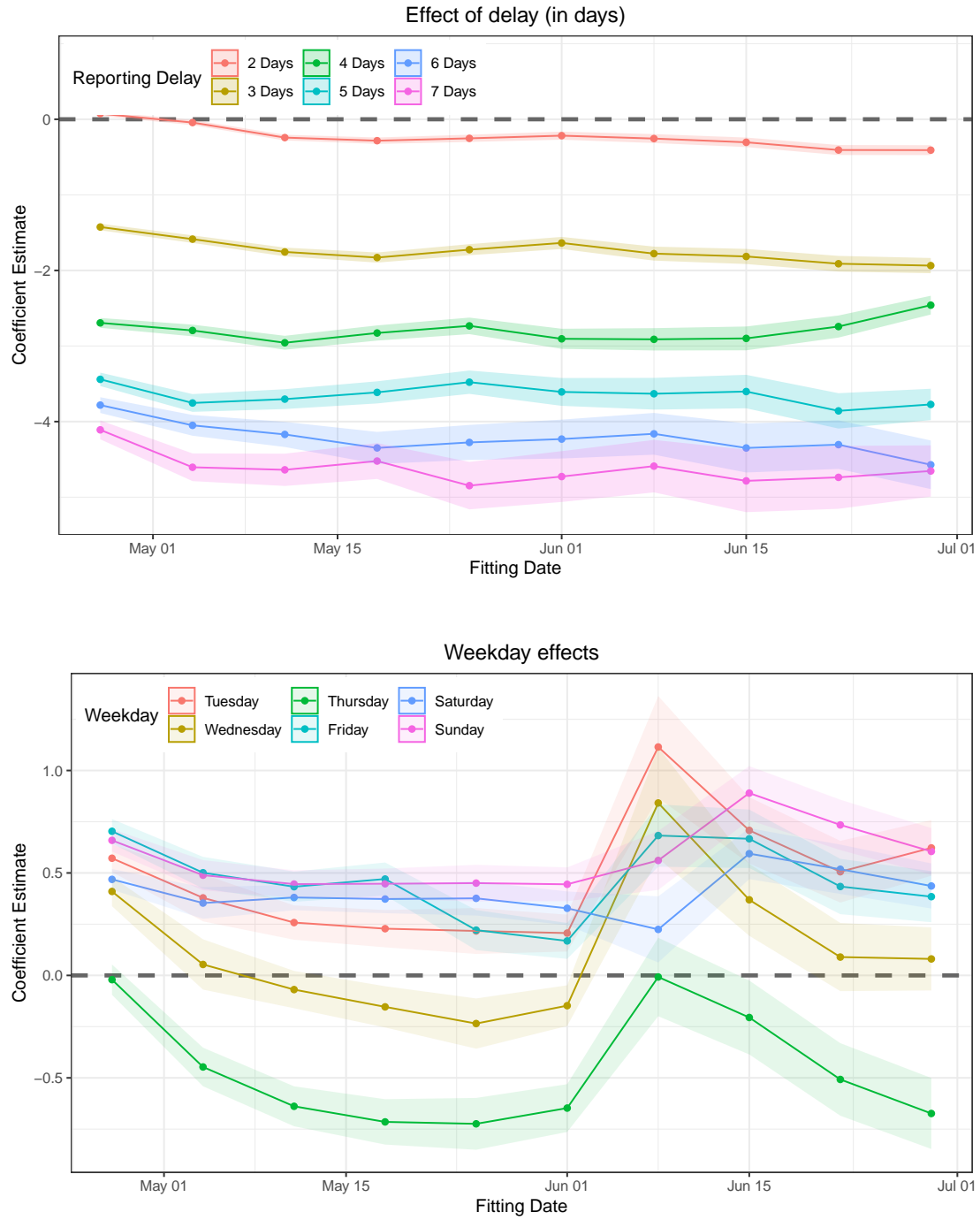


Figure 11: Estimated effects of the reporting-related components of the model over time. The dashed zero-line corresponds to the effect of the reference category (reporting delay of 1 day and Monday, respectively).